
Coronary centerline tracking in CT images with use of an elastic model and image moments

Release 1.02

Marcela Hernández Hoyos¹, Maria A. Zuluaga^{1,2},
Mónica Lozano¹, Juan C. Prieto¹, Philippe C. Douek²,
Isabelle E. Magnin² and Maciej Orkisz²

July 25, 2008

¹Grupo Imagine, Grupo de Ingeniería Biomédica, Universidad de los Andes, Bogota, Colombia
marc-her@uniandes.edu.co

²Université de Lyon; Université Lyon 1; INSA-Lyon; CNRS UMR 5220, CREATIS; Inserm U630;
F-69621 Villeurbanne, France
maciej.orkisz@creatis.insa-lyon.fr

Abstract

This coronary-artery extraction method uses one initialization point per vessel. First, a mask is computed by use of a region-growing algorithm, which starts from the initial point and stops when no more connected voxels fall within an interactively defined intensity range. The centerline tracking is then performed within the mask, starting from the same initial point. This algorithm is based on a prediction/estimation scheme. It uses the first- and second-order image moments calculated within a spherical volume that slides along the vessel, and the radius of which is automatically adjusted to the local radius of the vessel. The evolution of the radius of the sphere is based on the analysis of the eigenvalues of the inertia matrix in a multi-scale framework. The estimation of the current point location makes use of an elastic model similar to "snakes". The point iteratively moves under the action of an image-force attracting it to the local gravity center, and under the reaction of the internal forces of the model, which reflect its shape constraints: continuity and smoothness. The prediction makes use of the eigenvectors of the inertia matrix. The stopping criteria of the centerline tracking are based on the size of the sphere and on the percentage of the masked voxels within the sphere.

On 8 training CT datasets, the following mean results were obtained. Overlap with reference: considering the whole length (OV) 80.1%, until the first failure (OF) 48.9%, in clinically relevant segments (radius > 1.5 mm, OT) 81.7%. Average distance from reference: considering the whole length (AD) 4.32 mm, limited to segments where the semiautomatic centerline remains within the vessel (AI) 0.39 mm, in clinically relevant segments (AT) 4.13 mm. On 16 testing datasets, these results were respectively: OV = 80.2%, OF = 39.3%, OT = 82.1%, AD = 5.05 mm, AI = 0.41 mm and AT = 4.58 mm. A number of failures was due to the fact that the model does not handle the bifurcations.

Latest version available at the [Insight Journal](http://hdl.handle.net/1926/1401) [<http://hdl.handle.net/1926/1401>]
Distributed under [Creative Commons Attribution License](#)

Contents

1	Method	2
1.1	Image preprocessing	3
1.2	Centerline-tracking algorithm	3
	Estimation of the current point location	3
	Estimation of the local orientation and prediction of the next centerline point	4
	Stopping criteria	4
1.3	Algorithm summary and parameter settings	4
2	Results	5
3	Discussion and conclusion	5

This paper describes a method submitted to the first Coronary Artery Tracking contest (CAT08) held in conjunction with the MICCAI 2008 conference <http://miccai2008.rutgers.edu/>.

Coronary artery disease remains one of the leading causes of death each year. Therefore, the evaluation of these vessels is of critical importance. Although manual delineation is still used in clinical routine, automatic and semiautomatic segmentation is necessary to decrease human effort and variability.

The existing methods for the extraction of coronary arteries pathways usually combine intensity criteria with some model of the centerline alone or of the whole cylindrical shape. The intensities are either directly used to perform a presegmentation [11, 7], or to enhance the points likely to be located on the centerline. The latter makes use of models based on differential geometry (Hessian eigenanalysis) [9, 10] or mechanics (inertia moments) [1]. The centerline is often modeled by a minimal cost path [9]. Variants of this approach can be found in [7] (minimal Euclidean length path within a skeleton) and in [6]. The latter models a vessel by a union of spheres: the sphere centers define the vessel centerline, while the sphere radii represent the vessel local radii. Both are simultaneously determined by a minimum cost path search in a 4D space, where the additional 4-th dimension corresponds to the radius. A similar model based on spheres is used in [5], but the segmentation is carried out by use of a Bayesian approach inspired by particle filtering.

The main challenges still remain the managing of bifurcations, of severe stenoses and of adjacent hyperintense structures.

1 Method

The core of our method is a minimally interactive centerline-tracking algorithm (section 1.2). According to the definition given by the organizers of CAT08 <http://cat08.bigr.nl/> [8], a minimally interactive algorithm is "allowed to use one point per vessel as input". However, our algorithm was initially developed to be used in contrast-enhanced magnetic resonance images of carotid and peripheral arteries, and is based on the assumption that the vessels are high-intensity thread-like objects on low-intensity background. As this assumption is not met in CT images representing the coronary arteries, an interactive preprocessing step was added (section 1.1), which intends to remove as much background and surrounding structures as possible. The method was implemented in a software package called Maracas (Magnetic Resonance Angiography Computer Assisted Analysis <http://www.creatis.insa-lyon.fr/maracas/>).

1.1 Image preprocessing

The preprocessing is actually a coarse presegmentation that provides a connected set \mathcal{V}_{pre} of voxels, the intensities of which are likely to correspond to arteries or calcifications. A region-growing process is carried out starting from a user-defined seed point. Neighboring voxels are iteratively added to \mathcal{V}_{pre} as long as their intensity is above a threshold T_L . Starting from a preset value, the user can modify T_L , while visualizing the result in real time, in order to check whether the subset \mathcal{V}_{pre} contains the distal part of the vessel to be extracted, and to avoid the inclusion of too many neighboring structures.

1.2 Centerline-tracking algorithm

Hereafter, we give an overview of the algorithm. More details can be found in our previous publications [2, 3]. The algorithm extracts the centerline of one vessel of interest, starting from a point within its lumen, the same one that was previously used to initialize the preprocessing. It includes the following steps:

- a) estimation (refinement) of the current point location \mathbf{x}_i , based on centroid information and restricted by continuity and smoothness constraints,
- b) estimation of the local orientation \mathbf{e}_i of the vessel, based on inertia matrix eigenvectors,
- c) prediction of the next (candidate) point $\hat{\mathbf{x}}_{i+1}$ based on the estimated location and orientation.

First- and second-order image moments used in the algorithm are computed within a spherical sub-volume called *analysis cell*. We use a multi-scale framework to determine the locally most suitable size of the cell. The iterative tracking process is carried out in two opposite directions from the starting point, and stops when one of the stopping criteria is encountered. In CT images of the coronary arteries, the tracking process is carried out within the subvolume masked by \mathcal{V}_{pre} , and the stopping criteria are related to the percentage of voxels within the analysis cell, falling into the expected intensity range.

Estimation of the current point location

Each centerline point is expected to coincide with the centroid of the analysis cell. However, to cope with noise, pathologies, nearby structures etc., we constrain the shape of the centerline by means of a model similar to the well-known "snakes". Starting from the predicted position $\mathbf{x}_i^0 = \hat{\mathbf{x}}_i$, the location \mathbf{x}_i^j of the current point is iteratively refined under the action of an image-based *external* force and the reaction of the *internal* forces of the model, as long as the resulting displacement is larger than a fixed minimum value. The *external* force attracts the point toward the centroid \mathbf{x}_i^G of the cell located in \mathbf{x}_i^j . The *internal* forces enforce the continuity and smoothness of the model, respectively weighted by coefficients w_c and w_s (see section 1.3 for the parameter values). At j -th iteration, the corrected location of the current point is:

$$\mathbf{x}_i^j = \mathbf{x}_i^{j-1} - \left(\mathbf{x}_i^{j-1} - \mathbf{x}_i^{G,j} \right) - w_c \left(\mathbf{x}_i^{j-1} - \mathbf{x}_{i-1} \right) - w_s \left(\mathbf{x}_i^{j-1} - 2\mathbf{x}_{i-1} + \mathbf{x}_{i-2} \right). \quad (1)$$

After stabilization of the position, the diameter of the analysis cell may need to be modified, in order to fit the local diameter of the vessel. Otherwise, when the cell is too small, its gravity center is not meaningful. Conversely, when the cell is too large it may contain fragments of neighboring structures that would modify the location of the gravity center. In pathologic regions, as well as near the branching points, abrupt changes of the local vessel diameter may be observed. Therefore, the diameter calculated at the previous centerline point is sometimes not suitable at the current point. To solve this problem, eigenvalues of the inertia matrix, calculated within the current cell, are analyzed to make evolve the cell size. When the cell is included within a vessel, its content has no privileged orientation and the inertia moments are identical for any axis.

Conversely, when the cell is large enough to contain a cylindrical portion of the vessel, there is only one axis, corresponding to the local orientation of the vessel, around which the cylinder would spin with minimum inertia moment. Finding the appropriate size of the cell is based on the detection of the limit between the spherical and cylindrical behavior of the structure contained within the cell. The adaptation of the size of the cell is carried out by "inflating" the cell as long as all three eigenvalues of the inertia matrix are approximately equal each to other, or by "deflating" it when the eigenvalues are significantly different. After each resizing the process moves back to the repositioning, if necessary, and so on. When both the position and the radius of the cell become stable, the latter, denoted by ρ_{opt} , is approximately equal to the radius of the vessel.

Estimation of the local orientation and prediction of the next centerline point

The local orientation of the vessel is defined by the eigenvector \mathbf{e}_i associated to the smallest eigenvalue of the inertia matrix of a cell centered in \mathbf{x}_i . The radius ρ_{pred} of the sphere used for this purpose is to be large enough to encompass a portion of the vessel of interest, and small enough so that this portion be considered as approximately straight cylinder. The best experimental results are obtained when the diameter of the cell is between 1.5 and twice the vessel diameter. The prediction is carried out along the eigenvector \mathbf{e}_i , with amplitude δ :

$$\hat{\mathbf{x}}_{i+1} = \mathbf{x}_i + \delta \mathbf{e}_i, \quad (2)$$

According to our experience, δ is to be set approximately equal to half the vessel radius.

Stopping criteria

Two criteria are defined to stop the tracking of an artery when reaching its proximal (aortic) or distal end, respectively. First, we analyze a sphere with a radius as large as $\rho_{max} = 15$ voxels, positioned at the current end-point of the centerline. This sphere is very likely to be included within the aorta if almost all the voxels within it have typical "arterial" intensities. If more than 90% of them belong to \mathcal{V}'_{pre} , we consider that the proximal (aortic) end of the coronary artery was reached. Second, if less than 30% of the voxels within the current analysis cell (i.e. with a radius adapted to the local size of the vessel and centered at the current end-point of the centreline) belong to \mathcal{V}'_{pre} , we consider that the distal end of the artery was reached.

1.3 Algorithm summary and parameter settings

Our method can be summarized as follows (see [4] for a detailed flowchart of the tracking algorithm):

- a) initialization: preset values of T_L and ρ_0 , interactively defined initial point \mathbf{x}_0 ,
- b) presegmentation: starting from \mathbf{x}_0 , build a connected set \mathcal{V}'_{pre} of points with intensities higher than T_L ;
- c) if T_L interactively modified, return to b);
- d) compute the centroid, eigenvalues and eigenvectors within the analysis cell (center \mathbf{x}_i^j , radius ρ_i^j);
- e) reposition \mathbf{x}_i^j according to eq. 1 as long as the displacement is larger than half voxel size;
- f) compare the eigenvalues, then increase or decrease ρ_i^j and return to d) if necessary;
- g) otherwise evaluate the stopping criteria and predict $\mathbf{x}_{i+1}^0 = \hat{\mathbf{x}}_{i+1}$ according to eq. 2, if end not reached;

The parameters of the model were empirically fixed as follows [2]: $w_c = 0.5$ (rather low elasticity), $w_s = 0.1$ (rather high flexibility). The estimation of the orientation and the prediction used the aforementioned ratios: $\rho_{pred} = 1.5\rho_{opt}$, $\delta = \rho_{opt}/2$. As for the intensity threshold used at the preprocessing step, the interactively adjusted values were on average: $T_L = 150 \pm 38$ HU.

Table 1: Average overlap per testing dataset

Dataset nr.	OV			OF			OT			Avg. rank
	%	score	rank	%	score	rank	%	score	rank	
8	70.8	38.6	–	38.4	28.8	–	72.6	36.4	–	–
9	88.6	45.9	–	64.3	40.2	–	89.7	57.3	–	–
10	67.4	34.4	–	40.4	20.6	–	70.3	47.7	–	–
11	91.5	59.3	–	49.5	39.4	–	91.6	59.4	–	–
12	84.0	43.4	–	7.5	3.8	–	88.6	44.6	–	–
13	81.7	41.4	–	23.4	11.7	–	83.3	54.2	–	–
14	84.7	42.9	–	22.8	14.3	–	85.2	42.6	–	–
15	90.8	46.4	–	86.3	57.0	–	93.1	59.1	–	–
16	84.8	55.2	–	54.3	40.1	–	89.3	57.2	–	–
17	64.6	37.5	–	9.5	5.3	–	66.6	34.8	–	–
18	76.4	38.7	–	69.5	56.7	–	77.4	51.3	–	–
19	79.5	41.2	–	63.1	34.5	–	79.6	39.8	–	–
20	62.9	40.6	–	14.2	7.3	–	63.4	31.8	–	–
21	91.2	46.4	–	18.1	10.0	–	95.5	48.2	–	–
22	71.8	36.2	–	60.7	30.4	–	75.2	37.6	–	–
23	91.8	46.4	–	6.8	3.4	–	91.8	45.9	–	–
Avg.	80.2	43.4	–	39.3	25.2	–	82.1	46.7	–	–

2 Results

The results hereafter described were obtained on 24 datasets of variable quality provided by the organizers of the contest: 8 of them were available at the training stage together with reference segmentations, while the remaining 16 were only used at the testing stage. The interactive presegmentation took several minutes per dataset, but this duration was highly dependent on image contrasts. The computational time of the centerline extraction was around 20 s on average, depending on the artery length. In each dataset the centerlines were extracted in four arteries: RCA, LAD, LCX and one large side branch. These centerlines were then compared to reference segmentations, according to the rules of the contest specified at the CAT08 web page <http://cat08.bigr.nl/> [8]. The reference segmentations were calculated based on centerlines and local radii manually delineated by three experts. The tracking capability of the method was assessed by three overlap measures (table 1): OV = overall, OF = until first failure, OT = in clinically relevant segments (radius > 1.5 mm), where the semi-automatic centerline was considered as overlapping wherever its distance to the reference centerline was less than the local radius. The accuracy was also assessed by three measures (table 2) based on the average distances between the centerlines: AD = on whole length, AI = inside the vessel (i.e. where the distance between the centerlines is less than the vessel radius), AT = in clinically relevant segments. The results obtained on the training and testing datasets were very similar and are respectively summarized in tables 4 and 3. Figure 1 shows an example of the centerlines extracted by our method (blue) superimposed onto the reference centerlines (white = RCA, yellow = LAD, green = LCX, red = diagonal branch of LAD). The corresponding average overlap and distance measures were as follows:

- dataset 4: OV = 81.1%, OF = 53.2%, OT = 85.0%, AD = 4.04 mm, AI = 0.36 mm, AT = 3.34 mm;
- dataset 6: OV = 88.6%, OF = 80.4%, OT = 89.5%, AD = 2.05 mm, AI = 0.32 mm, AT = 2.00 mm.

3 Discussion and conclusion

One of the principal difficulties is the detection of the distal end of the artery, where the limitations of image contrast and resolution are reached. The point annotated as artery end usually corresponds to the absence of signal rather than to the anatomic very end of the vessel. However, signal gaps may occur earlier on the arterial pathway, owing to stenoses, artifacts or noise. When our algorithm encounters a gap it stops, while a human expert is able to use his(her) anatomic knowledge in order to scan an appropriate region seeking for a

Table 2: Average accuracy per testing dataset

Dataset nr.	AD			AI			AT			Avg. rank
	mm	score	rank	mm	score	rank	mm	score	rank	
8	5.36	25.0	–	0.49	33.3	–	5.13	25.7	–	–
9	3.04	25.6	–	0.32	28.5	–	2.96	26.0	–	–
10	9.37	19.6	–	0.41	29.5	–	9.14	20.9	–	–
11	1.82	31.4	–	0.41	34.0	–	1.82	31.4	–	–
12	1.44	23.9	–	0.39	27.9	–	0.78	25.4	–	–
13	4.14	22.9	–	0.36	27.6	–	3.46	23.4	–	–
14	1.55	30.2	–	0.41	34.5	–	1.38	30.3	–	–
15	1.23	26.8	–	0.35	29.2	–	1.00	27.3	–	–
16	1.54	23.7	–	0.35	27.3	–	0.91	24.8	–	–
17	6.98	30.3	–	0.38	41.3	–	6.92	31.5	–	–
18	9.51	21.2	–	0.36	28.5	–	9.42	21.4	–	–
19	5.39	26.3	–	0.45	32.8	–	5.36	26.3	–	–
20	13.54	17.4	–	0.62	25.6	–	13.47	17.4	–	–
21	1.03	20.8	–	0.39	22.4	–	0.58	21.6	–	–
22	14.03	19.5	–	0.50	25.7	–	10.04	20.3	–	–
23	0.88	26.7	–	0.38	28.8	–	0.88	26.7	–	–
Avg.	5.05	24.5	–	0.41	29.8	–	4.58	25.0	–	–

Table 3: Summary of the results on the testing datasets

Measure	% / mm			score			rank		
	min.	max.	avg.	min.	max.	avg.	min.	max.	avg.
OV	20.5%	100.0%	80.2%	10.4	100.0	43.4	–	–	–
OF	0.0%	100.0%	39.3%	0.0	100.0	25.2	–	–	–
OT	27.9%	100.0%	82.1%	14.0	100.0	46.7	–	–	–
AD	0.31 mm	48.93 mm	5.05 mm	4.9	47.7	24.5	–	–	–
AI	0.24 mm	0.89 mm	0.41 mm	16.5	63.8	29.8	–	–	–
AT	0.25 mm	36.18 mm	4.58 mm	7.1	51.9	25.0	–	–	–
Total							–	–	–

Table 4: Summary of the results on the training datasets

Measure	% / mm			score			rank		
	min.	max.	avg.	min.	max.	avg.	min.	max.	avg.
OV	36.5%	99.4%	80.1%	19.8	78.2	43.0	–	–	–
OF	0.0%	100.0%	48.9%	0.0	100.0	32.8	–	–	–
OT	36.5%	100.0%	81.7%	18.7	100.0	47.2	–	–	–
AD	0.30 mm	19.54 mm	4.32 mm	12.6	39.2	25.0	–	–	–
AI	0.24 mm	0.67 mm	0.39 mm	23.4	42.6	30.8	–	–	–
AT	0.29 mm	19.54 mm	4.13 mm	12.8	39.2	25.3	–	–	–
Total							–	–	–

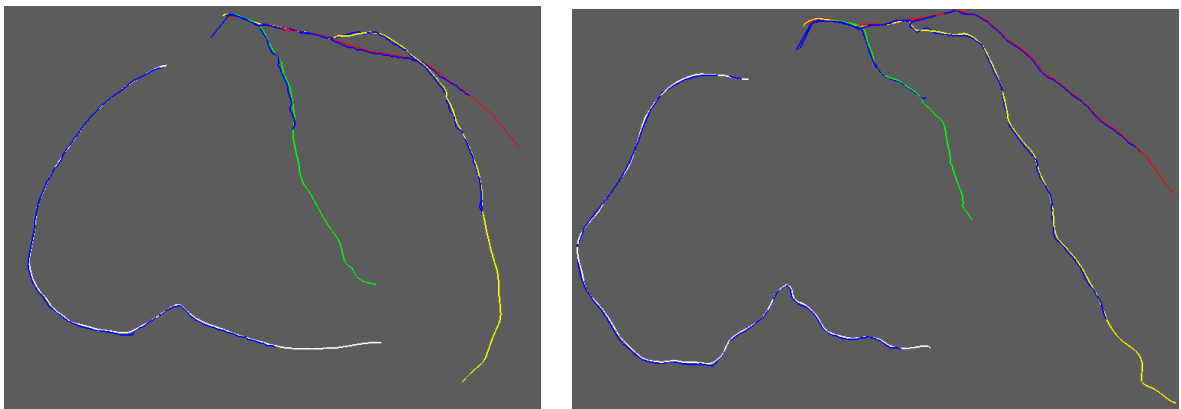


Figure 1: Examples of centerlines obtained with our method (blue) superimposed onto the reference centerlines (white = RCA, yellow = LAD, green = LCX, red = diagonal branch of LAD): datasets 4 (left) and 6 (right).

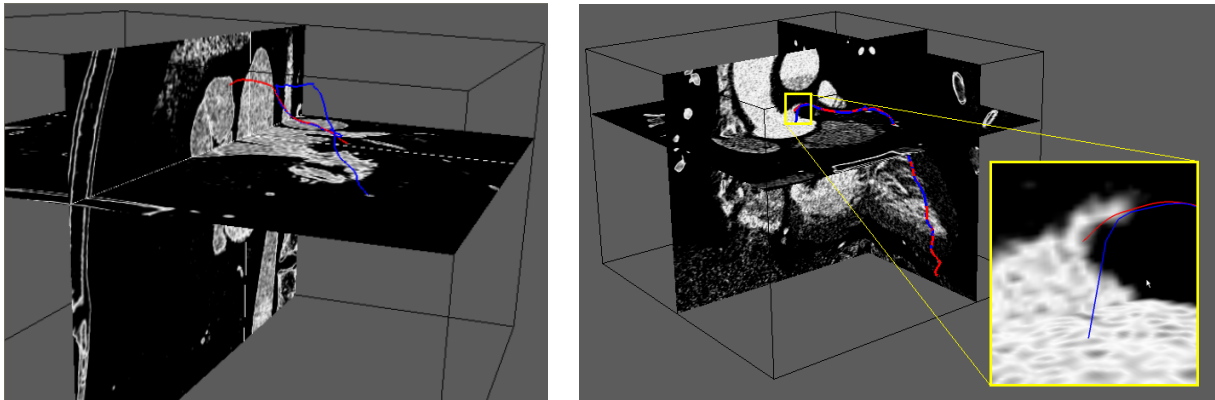


Figure 2: Examples of failures. Left (dataset 06, LCX): the semiautomatic centerline (blue) correctly follows the reference one (red) in the LCX until it reaches the common trunk of the LCA, then it turns toward the distal part (LAD), thus failing to reach the aorta. Right (dataset 1, LAD): while the overall overlap between blue and red centerlines is good $OV = 91.4\%$, the semi-automatic centerline makes a "shortcut" toward the high-intensity interior of the aorta, which results in $OF = 0.0\%$.

possible continuation of the artery. For this reason, the presegmentation step is to be done very carefully and appears to be time-consuming. One possible perspective to improve our method is to include some anatomic prior and to mimic the expert's reasoning.

Despite this limitation, the overall tracking capability (OV) of our algorithm is quite good. However, the average scores for OF were low, owing to several vessels with $OF = 0.0\%$, which means that the very first point of such centerlines is not correctly located on the boundary of the aorta. This occurs in two situations.

The first one (fig. 2 left) can be explained by the fact that our model does not manage bifurcations. When a centerline initialized in a secondary branch (e.g. LCX or diagonal branch of LAD) reaches the primary branch, it may turn toward its distal (instead of proximal) part, and thus never reach the aorta. Once again, the addition of some anatomic prior might avoid this kind of errors.

In the second situation (fig. 2 right) the very last point of the centerline is strongly attracted by the aorta, since the gravity center falls within this large hyperintense structure. The analysis cell grows trying to adapt itself to the sudden change of vessel size. Consequently, the gravity center iteratively moves further into the aorta toward its most intense part, which is not necessarily in front of the coronary artery. We will intend to solve this problem by adaptively increasing the coefficients w_c and w_s of the model whenever a sudden increase of the analysis-cell radius will be detected. Let us note that in both situations the centerline might be easily corrected by interactively placing an additional point. However, we refrained ourselves from other interaction than the initial adjustment of the thresholds and the definition of one starting point per artery.

As for the accuracy, the average scores were rather low. We identified two sources of large errors: 1) in bifurcations the algorithm sometimes "hesitates" between the two branches, 2) in calcified regions the centerline is attracted by the hyperintense plaque. While the first of these problems is likely to be solved by a relatively simple postprocessing of the centerline, the latter requires a more careful design. Beyond the bifurcations and calcified regions, we frequently observed that the semi-automatic centerline was parallel to the reference one at approximately one-voxel distance. This may be a numerical implementation problem.

In conclusion, our method requires the following interaction: initial adjustment of an intensity threshold and placement of one starting point per artery. The first of them is sometimes time-consuming and needs to be replaced by a more automated process, while the subsequent extraction of the centerlines is fast. The

tracking capability of the algorithm is satisfactory and still can be improved, either by the aforementioned modifications of the algorithm, or by additional interaction. The accuracy is less satisfactory and requires a careful revision of the model and of the implementation.

Acknowledgments

Work supported by ECOS-Nord #C07M04 and Region Rhône-Alpes PP3/I3M of cluster ISLE.

References

- [1] J.F. Carrillo, M. Hernández Hoyos, E.E. Dávila, and M. Orkisz. Recursive tracking of vascular tree axes in 3D medical images. *Int J Comp Assisted Radiol Surg*, 1(6):331–339, 2007. ([document](#))
- [2] M. Hernández Hoyos, M. Orkisz, P.C. Douek, and I.E. Magnin. Assessment of carotid artery stenoses in 3D contrast-enhanced magnetic resonance angiography, based on improved generation of the centerline. *Mach Graphics Vision*, 14(4):349–378, 2005. [1.2](#), [1.3](#)
- [3] M. Hernández Hoyos, P. Orłowski, E. Piątkowska-Janko, P. Bogorodzki, and M. Orkisz. Vascular centerline extraction in 3D MR angiograms for phase contrast MRI blood flow measurement. *Int J Comp Assisted Radiol Surg*, 1(1):51–61, 2005. [1.2](#)
- [4] M. Hernández Hoyos, J.M. Serfaty, A. Maghiar, C. Mansard, M. Orkisz, I.E. Magnin, and P.C. Douek. Evaluation of semi-automatic arterial stenosis quantification. *Int J Comp Assisted Radiol Surg*, 1(3):167–175, 2006. [1.3](#)
- [5] D. Lesage, E.D. Angelini, I. Bloch, and G. Funka-Lea. Medial-based bayesian tracking for vascular segmentation: Application to coronary arteries in 3D CT angiography. In *5th IEEE Int Symp Biomed Imaging*, pages 268–271, Paris, France, May 2008. ([document](#))
- [6] H. Li and A. Yezzi. Vessels as 4D curves: Global minimal 4D paths to extract tubular surfaces. In *Computer Vision and Pattern Recognition Workshop*, 2006. ([document](#))
- [7] C. Metz, M. Schaap, A. van der Giessen, T. van Walsum, and W. Niessen. Semi-automatic coronary artery centerline extraction in computed tomography angiography data. In *4th IEEE Int Symp Biomed Imaging*, pages 856–859, Washington, DC, USA, April 2007. ([document](#))
- [8] C. Metz, M. Schaap, T. van Walsum, A. van der Giessen, A. Weustink, N. Mollet, G. Krestin, and W. Niessen. 3d segmentation in the clinic: A grand challenge ii - coronary artery tracking. *Insight Journal*, 2008. [1](#), [2](#)
- [9] S.D. Olabarriaga, M. Breeuwer, and W.J. Niessen. Evaluation of hessian-based filters to enhance the axis of coronary arteries in ct images. In *Comp Assisted Radiol Surg*, volume 1256 of *Int Congress Series*, pages 1191–1196. Elsevier, 2003. ([document](#))
- [10] F. Renard and Y. Yang. Image analysis for detection of coronary artery soft plaques in MDCT images. In *5th IEEE Int Symp Biomed Imaging*, pages 25–28, Paris, France, May 2008. ([document](#))
- [11] S. Wesarg and E.A. Firle. Segmentation of vessels: The corkscrew algorithm. In J.E. Robert L. Galloway, editor, *Proc SPIE Int Symp Med Imaging*, volume 5370, pages 1609–1620, San Diego, California, February 2004. ([document](#))